Reports

Volcanic Aerosols and Lunar Eclipses

Abstract. *The moon is visible during total lunar eclipses due to sunlight refracted into the earth's shadow by the atmosphere. Stratospheric aerosols can profoundly affect the brightness of the eclipsed moon. Observed brightnesses of 21 lunar eclipses during 1960–1982 are compared with theoretical calculations based on refraction by an aerosol-free atmosphere to yield globally averaged aerosol optical depths. Results indicate the global aerosol loading from the 1982 eruption of El Chichón is similar in magnitude to that from the 1963 Agung eruption.*

Total lunar eclipses, which occur when the moon passes completely into the earth's shadow, happen on the average of about once a year. As suggested by Kepler (*1*), the moon is visible during the eclipse because sunlight is refracted (and to a much lesser extent, scattered) into the shadow by the earth's atmosphere. Rays of sunlight passing between 5 and 25 km above the earth's surface are most effective at illuminating the eclipsed moon. The brightness of the moon will be affected by the refractive properties of this layer, the presence of absorbing media such as clouds, ozone, and aerosols in and above the layer, and the position of the moon within the shadow. Large differences in brightness between eclipses have been noted for centuries. The *Anglo-Saxon Chronicle* (*2*) describes an exceptionally dark eclipse in 1110, and Kepler attributed the near disappearance of the moon during an eclipse in 1588 to mists and smoke in the earth's atmosphere. The volcanic origin of these aerosols became apparent when a series of dark eclipses followed the 1883 eruption of Krakatoa (*3*), and most other dark eclipses since 1600 have subsequently been linked to major eruptions (*4, 5*). Comparing Link's (*6*) theory with photometric observations of the distribution of light within the earth's shadow for three eclipses following the 1963 Agung eruption, Matsushima *et al.* (*7, 8*) derived global average extinction coefficients for the volcanic aerosol veil.

The observational requirements can be simplified by using Link's theory (modified by assumed distributions of clouds and ozone) to compute the integrated brightness of the totally eclipsed moon. These theoretical brightnesses are compared with observations of 21 eclipses between 1960 and 1982; the differences (observed minus calculated) are presumed to be largely due to stratospheric aerosols, for which an estimate of global content is made for each eclipse.

Ray equations including the effects of refraction, absorption, and scattering in pure molecular atmosphere are defined by Link (*6*) for three standard wavelengths (0.46, 0.54, and 0.62 μm). Assuming the earth's atmosphere to be symmetric about the shadow axis, Link integrates the equations over height above the earth's surface and the area of the solar disk to arrive at a three-dimensional distribution of light in the earth's shadow. In this report, results for the three standard wavelengths are averaged according to the response of the dark-adapted human eye (*9*) for comparison with visual observations. Further integration over the area occupied by the moon yields a brightness of the eclipsed moon that depends on the moon's distance from both the earth and the shadow axis during the particular eclipse (*10*). These integrations are modified by an assumed line-of-sight blocking effect of clouds with an effective optical depth that decreases linearly from 1 for rays grazing the earth's surface to 0 at an altitude of 10 km. The darkening effect (in equivalent optical depths) of this cloud distribution on the eclipsed moon ranges from 0 for a total eclipse located near the edge of the shadow to 0.6 for a central eclipse. A nearly constant line-of-sight absorption of $\tau \approx 0.5$ due to a high ozone layer (*6*) is adopted.

The calculated brightness B_c of the eclipsed moon is expressed as an attenuation τ_c of the brightness of the uneclipsed full moon B_f (*11*); thus,

$$\tau_c = -\ln(B_c/B_f)$$

The temporal standard deviations of atmospheric density (that is, refractive index) in the 5- to 25-km layer are everywhere less than 0.05 of the mean (*12*) and therefore are not expected to contribute much to variability of eclipse brightness. The contribution from clouds and ozone to τ_c are each on the order of 0.5; the combined standard deviation of these factors should be less than this value. Therefore, the probable error of τ_c due to varying factors that are held constant may be considered to be less than 0.5.

Published observations of the moon's brightness at mideclipse (*13–17*) supplemented by the author's observations (*18*), are available for all 21 total lunar eclipses between 1960 and 1982. As was done for B_c the observed brightness B_o is expressed as τ_o, where

$$\tau_o = -\ln(B_o/B_f)$$

Direct brightness measurements for 15 of the eclipses have an estimated average probable error of ±0.3. Brightnesses for the other six eclipses are derived from the appearance of the eclipsed moon (color and visibility of surface features) and have a probable error of ±0.8 (*19*).

Elevated values of the observed minus calculated attenuation of brightness (τ_{o-c}), presumably due to volcanism, occur for ten eclipses: those between 1963 and 1968, the one in May 1975, and those in July and December 1982. The average value of τ_{o-c} for the other 11 eclipses is 0.7; the same average is found for seven eclipses during the volcanically quiet period from 1924 through 1942. This background attenuation may be due to background aerosols or to systematic (but constant) errors in the assumptions

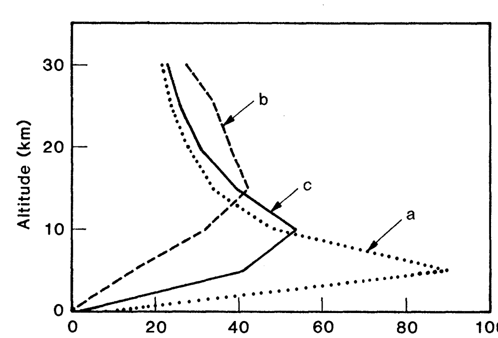

Fig. 1. Optical depth factor L for globally and vertically uniform 5-km-deep aerosol layers based at the altitude indicated. L is computed for (a) an eclipse centered on the shadow axis, (b) one at the edge of the shadow, and (c) an "average" eclipse (for example, January 1982).

behind τ_c. In either case, subtracting the background value from τ_{o-c} yields an attenuation that may be attributed to specific volcanic events. Assuming a uniform global distribution of aerosols, the zenithal optical thickness τ_z of the layer may be computed as

$$\tau_z = (\tau_{o-c} - 0.7)/L$$

where L is the ratio of the mean path-length through the layer to the vertical depth of the layer for rays illuminating the moon. Values of L range from 25 to 60 for various plausible stratospheric aerosol layers (Fig. 1). Upper tropospheric (5 to 10 km) aerosols may affect the moon's brightness, particularly during central eclipses; however, these aerosol layers are usually short-lived. Lower tropospheric (0 to 5 km) aerosols should have little effect. An L value of 40, corresponding approximately to a vertically uniform layer between 15 and 20 km, is adopted for scaling Table 1 and Fig. 2. The uncertainty in the derived values of τ_z due to the estimated errors in τ_o and τ_c is ± 0.01 ($\pm$ 0.02 for τ_z derived from descriptive observations).

Interpretation of the derived τ_z is complicated somewhat by the differing paths of the moon through the shadow for different eclipses. The eclipses in Table 1 are classified by whether the lunar disk passed entirely north or south of the shadow axis or whether some portion of the disk crossed the shadow center. For any total lunar eclipse, some contribution to the illumination will come from every latitudinal segment of the earth's limb; however, for a north or south eclipse path this illumination will be weighted toward the respective terrestrial hemisphere (*20*). Therefore, the derived τ_z for a north or south eclipse path may be considered a global average weighted toward the indicated hemisphere, whereas for a central eclipse path, τ_z is a more uniform global average value.

Sudden increases of τ_z are noted following the eruptions of Agung (1963), Fernandina (1968), Fuego (1974), and El Chichón (1982). The small increase of τ_z for the September 1979 eclipse, while near the uncertainty level, may indicate effects of the eruption of La Soufrière of Saint Vincent 5 months earlier. Comparative maximum values of τ_z following Agung (0.13), Fernandina (0.06), and Fuego (0.04) agree well with the relative aerosol loadings for the three events indicated by smoothed Mauna Loa transmission values (*21*) and by Lamb's dust veil indices (*22*). The derived values of τ_z for three eclipses in 1963 and 1964 closely agree with those determined by Matsushima *et al.* (*7, 8*).

The December 1982 eclipse was 9 months after the eruption of El Chichón, as was the darkest eclipse after the eruption of Agung; also, both eclipses were weighted toward the hemisphere with the greater aerosol concentration. Therefore, the derived τ_z of 0.12 for the December 1982 eclipse can be compared directly with that for the December 1963 eclipse. It should be noted that in both cases τ_z may be slightly (10 to 20 percent) underestimated because of the relatively high (20 to 25 km) altitude of the main aerosol layers (*23, 24*). These results indicate that the global aerosol loading from El Chichón (and other 1982 eruptions) is similar in magnitude to that from Agung and (by analogy with Agung) will be half as much by the end of 1983, and decrease to zero during 1985. The intermediate value of τ_z in July 1982 reflects the incomplete dispersion of the aerosols only 3 months after the eruption of El Chichón. The concentration of aerosols over the Northern Hemisphere during July 1982 was apparent in the uneven illumination of the moon during that month's eclipse, with the northern portion of the eclipsed moon being perceptibly darker than the southern portion (*25, 26*).

In summary, observations of lunar eclipse brightnesses can be used to provide instantaneous measures of globally averaged aerosol absorption. The drawbacks of the technique are the irregular occurrence of eclipses and the necessary

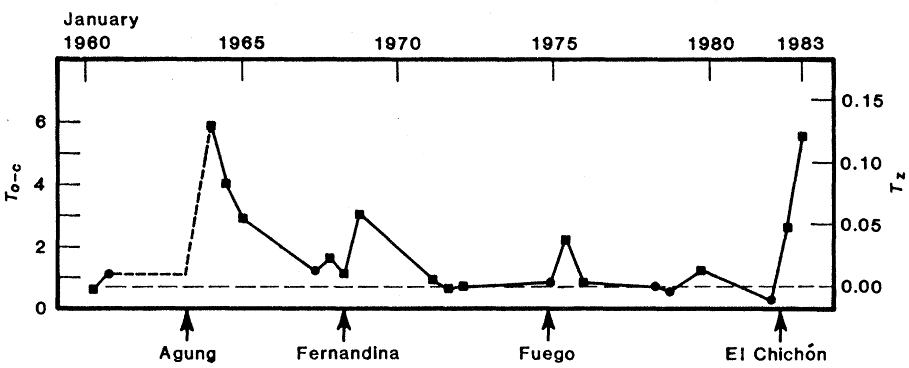

Fig. 2. Volcanic aerosol loading estimates obtained from observations of 21 lunar eclipses between 1960 and 1982. Global average optical depths (right-hand scale) are derived from observed minus calculated eclipse brightnesses (left-hand scale). Probable errors are ± 0.01 for values of τ_z plotted as squares and ± 0.02 for τ_z plotted as dots.

Table 1. Derivation of global average volcanic aerosol optical depth τ_z from lunar eclipse brightnesses. Visual stellar magnitude observations (m_v) are converted to equivalent attenuations (τ_o) of the full moon brightness and are compared with the theoretical attenuation (τ_c). The observed minus calculated (τ_{o-c}) are primarily due to volcanic aerosols and are reduced to τ_z in the last column. N, C, and S indicate the position (north, central, or south) of the moon in the earth's shadow.

Date	Position	m_v	Reference	τ_o	τ_c	τ_{o-c}	τ_z
13 March 1960	C	−0.9	(*13*)	10.9	10.3	0.6	0.00
5 September 1960	C	−0.5*	(*13*)	11.3	10.2	1.1	0.01
30 December 1963	S	+4.1	(*13, 18*)	15.7	9.8	5.9	0.13
25 June 1964	C	+2.7	(*14*)	14.1	10.1	4.0	0.08
19 December 1964	N	+0.1	(*13, 18*)	12.0	9.1	2.9	0.05
24 April 1967	N	−0.8*	(*13*)	11.1	9.9	1.2	0.01
18 October 1967	S	−1.5	(*13*)	10.2	8.6	1.6	0.02
13 April 1968	S	−2.2	(*13*)	9.8	8.8	1.0	0.01
6 October 1968	N	+0.1†	(*13*)	11.8	8.8	3.0	0.06
10 February 1971	N	−1.6	(*13*)	10.1	9.3	0.8	0.00
6 August 1971	C	+0.1†	(*15*)	11.9	11.3	0.6	0.00
30 January 1972	S	−3.0	(*13*)	8.9	8.2	0.7	0.00
29 November 1974	N	−1.7*	(*13*)	10.2	9.4	0.8	0.00
25 May 1975	C	+0.7	(*13, 18*)	12.3	10.1	2.2	0.04
18 November 1975	S	−2.9	(*13*)	9.0	8.2	0.8	0.00
24 March 1978	C	−1.0*	(*13*)	10.8	10.1	0.7	0.00
16 September 1978	N	−1.7*	(*13*)	10.2	9.7	0.5	−0.01
6 September 1979	S	−2.0	(*16*)	10.0	8.8	1.2	0.01
9 January 1982	S	−2.0*	(*17*)	10.0	9.8	0.2	−0.01
6 July 1982	C	+1.3	(*13, 18*)	12.8	10.2	2.6	0.05
30 December 1982	N	+2.9	(*13, 18*)	14.6	9.1	5.5	0.12

*Derived from descriptive appearance of eclipse. †Adjusted to mideclipse by applying theoretical brightness difference to observations made before or after mideclipse.

assumption of uniform aerosol distribution; the main advantage is that the optical property (τ) of most interest to atmospheric scientists is directly indicated. This technique has been applied to 21 eclipses to yield a comparison of four (possibly five) volcanic aerosol events between 1960 and 1982. It may be possible to extend the τ_z time series back to 1600 A.D. (*27*). A long time series of global aerosol loading could be compared with time series based on historic and geologic eruption records and ice cores.

RICHARD A. KEEN
Cooperative Institute for Research in Environmental Sciences, University of Colorado, Boulder 80309

References and Notes

1. J. Kepler, *Astronomiae Pars Optica* (Marnium & Aubrii, Frankfurt, 1604), pp. 267–284.
2. J. Ingram, translator, *The Anglo-Saxon Chronical* (Dutton, New York, 1913), pp. 187–188.
3. C. Flammarion, *L'Astronomie* **3**, 401 (1884).
4. F. Link, *Stud. Geophys. Geod.* **5**, 64 (1961).
5. P. Hédervári, *J. Assoc. Lunar Planet. Obs.* **28**, 158 (1980).
6. F. Link, *Eclipse Phenomena in Astronomy* (Springer-Verlag, New York, 1969), pp. 1–121.
7. S. Matsushima, J. R. Zink, J. E. Hansen, *Astron. J.* **71**, 103 (1966).
8. S. Matsushima, *Publ. Astron. Soc. Pac.* **79**, 178 (1967).
9. C. W. Allen, *Astrophysical Quantities* (Athlone, London, 1963), p. 105.
10. The geometric circumstances for eclipses are published annually in the *American Ephemeris and Nautical Almanac* (Government Printing Office, Washington, D.C., 1960–1980) and the *Astronomical Almanac* (Government Printing Office, Washington, D.C., 1981–1982).
11. The full moon's brightness varies slightly (*9*, pp. 144–146).
12. A. Oort and E. Rasmusson, *Atmospheric Circulation Statistics* (Government Printing Office, Washington, D.C., 1971), pp. 95–96.
13. Observation reports usually appear in *Sky and Telescope* 2 or 3 months after the date of the eclipse
14. A. Feinstein, *Bull. Astron. Inst. Czech.* **17**, 163 (1966).
15. H. J. Schober and A. Schroll, *Icarus* **20**, 48 (1973).
16. J. Westfall, *J. Assoc. Lunar Planet. Obs.* **28**, 116 (1980).
17. W. Haas, *ibid.* **29**, 128 (1982).
18. My visual magnitude estimates for five eclipses: 30 December 1963, +4.0; 19 December 1964, 0.0; 25 May 1975, +1.0; 6 July 1982, +0.7; and 30 December 1982, +2.5.
19. Many observers classify the appearance of lunar eclipses according to a five-category luminosity scale devised by A. Danjon [see (*6*), p. 97]. For the six eclipses for which direct brightness observations are not available, published luminosity values have been converted into visual magnitudes by an empirical relation derived from the other 15 eclipses.
20. The hemispheric weighting of illumination is graphically illustrated by imagery of the earth eclipsing the sun as seen by Surveyor III on the moon during the lunar eclipse of 24 April 1967. [E. Cortright, *Exploring Space with a Camera* (NASA SP-168, Government Printing Office, Washington, D.C., 1968), p. 128.]
21. B. G. Mendonca, K. J. Hanson, J. J. DeLuisi, *Science* **202**, 513 (1978).
22. H. Lamb, *Climate: Present, Past, and Future* (Methuen, London, 1972), vol. 1, p. 435.
23. F. E. Volz, *Science* **144**, 1121 (1964).
24. L. McClelland, J. Crampton, E. Nielson, *Sci. Events Alert Network (SEAN) Bull.* **8**, 8 (1983).
25. *Sky and Telescope* **64**, 390 (1982).
26. J. Westfall, *J. Assoc. Lunar Planet. Obs.* **29**, 168 (1982).
27. Any information on observations of eclipses prior to 1960 would be gratefully appreciated.
28. I thank Dr. Uwe Radok for his comments and encouragement.

27 June 1983; accepted 30 August 1983

Barium Isotopes in Allende Meteorite: Evidence Against an Extinct Superheavy Element

Abstract. *Carbon and chromite fractions from the Allende meteorite that contain isotopically anomalous xenon-131 to xenon-136 (carbonaceous chondrite fission or CCF xenon) at up to 5 × 10^{11} atoms per gram show no detectable isotopic anomalies in barium-130 to barium-138. This rules out the possibility that the CCF xenon was formed by in situ fission of an extinct superheavy element. Apparently the CCF xenon and its carbonaceous carrier are relics from stellar nucleosynthesis.*

Primitive meteorites contain a peculiar xenon component that is enriched up to twofold in the heavy isotopes ^{131}Xe to ^{136}Xe (*1*). The isotopic pattern resembles that of xenon from fission of actinides, and so this component has become known as CCF (carbonaceous chondrite fission) xenon. A possible source is an extinct superheavy element from the hypothetical "island of stability" (*2*) centered on the doubly magic nucleus ^{298}114 (*3*). An alternative possibility is direct nucleosynthesis of the heavy xenon isotopes, by neutron capture (*r*-process) in a supernova (*4, 5*).

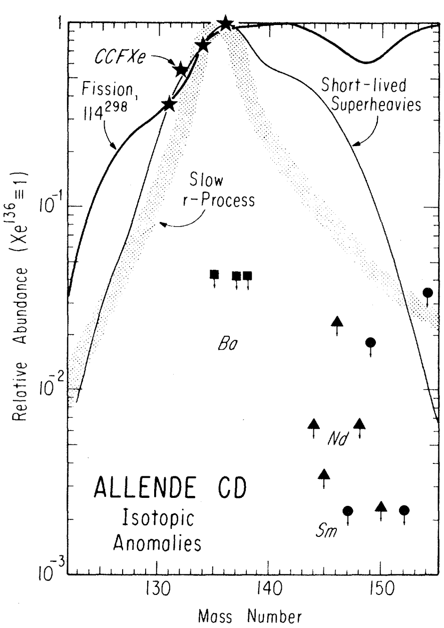

Fig. 1. Etch fractions from Allende CD that are highly enriched in CCFXe show no detectable anomalies for the neighboring elements Ba, Nd, and Sm. Upper limits range from 0.002 to 0.03 times the number of anomalous ^{136}Xe atoms, much less than predicted by the two principal models: in situ fission of a long-lived superheavy element (*7*) such as ^{298}114 (*17*), or neutron capture in stars (*4*), yielding nuclides near mass 140 either by direct buildup in a slow *r*-process (*5*) or by fission of short-lived superheavy elements of mass near 280 (*17*). Any process that made xenon isotopes 134 and 136 should have made comparable amounts of barium-135 to barium-138. The neutron capture model can escape this predicament by assuming that the Ba, Nd, and Sm expelled from the star condensed in the first crop of dust grains (oxides), whereas Xe condensed in a later crop (carbon). No such excuse is available for the in situ fission model, which is therefore ruled out by these data.

Until now, these two hypotheses have remained in a virtual stalemate (*6*). The fission model is supported by the correlation of CCFXe with volatile elements (*7, 8*), but it must invoke rather contrived explanations for the localization of CCFXe in a minor (~ 0.05 percent) carbon fraction in the meteorite (*8, 9*), and for its close coupling with another anomalous xenon component (L-Xe), enriched in isotopes 124 to 130 (*4*). The nucleosynthesis model can, in principle, account for these two trends, but has trouble explaining why the carbonaceous carrier of CCFXe is isotopically normal (*6, 9*), or why CCFXe is not accompanied by large amounts of ^{129}Xe from the decay of ^{129}I, of half-life 15 × 10^6 years (*10*).

An obvious test of both models had become feasible since the discovery of the carrier of CCFXe (*8*): detection of isotopic anomalies in neighboring elements, especially Ba and the light rare earth elements (REE) (*11*). With additional data points in the mass range 130 to 154, the isotopic pattern may be sufficiently well defined for a conclusive match or mismatch. However, the expected anomalies are on the order of 10^{11} atoms per gram of carrier, and hence require samples of very low Ba and REE content as well as careful chemistry and mass spectrometry. An early attempt gave negative but inconclusive results (*11*).

We prepared a sample strongly enriched in CCFXe by dissolving a large piece of the Allende C3V chondrite in HF-HCl, and removing noncolloidal material—mainly spinel—from the carbonaceous, acid-insoluble residue (*12*). We then treated this sample (Allende CD) with successively stronger oxidants to dissolve its main phases: (i) Q, the carrier of the dominant, normal xenon component (probably not a true phase, but merely an adsorbed surface layer); (ii) Cγ, gas-poor carbon; (iii) Cδ, gas-rich, resistant carbon, containing most of the CCFXe, and (iv) chromite (*9*) (Table 1). Barium, neodymium, samarium, and strontium were measured in the solu-